Sensors and Materials, Vol. 34, No. 9 (2022) 3479–3489
MYU Tokyo

S & M 3054

Analysis of Stator Material for Eliminating Cogging Torque

Ming-Jen Huang and Chia-Hung Lin*

Department of Electrical Engineering, National Kaohsiung University of Science and Technology,
415 Jiangong Rd., Sanmin Dist., Kaohsiung City 80778, Taiwan

(Received March 29, 2022; accepted June 21, 2022)

Keywords: cogging torque, nano Fe_3O_4 powder, hysteresis loop, permanent magnet brushless motor

Eliminating or reducing cogging torque has been the most important issue in the development of permanent magnet brushless motors. Because of the structure of the motor, the stator is traditionally made of a silicon steel plate with a copper wire winding, while the rotor silicon steel plate is clamped with a permanent magnet. Usually, when the power is off, the relative motion of the stator's silicon steel plate and the rotor's magnet produces cogging torque. This phenomenon affects the motor's smooth rotation and shortens the motor's life. In this paper, on the basis of the book Inventor-style Task-solving Theory (TRIZ) by the Soviet inventor Altshuller, we analyze the effect of the matter field on components or subsystems of interest, such as the components requiring improvement or with the lowest functional value in the system, or when a quick and simple model is required to provide a designer with a different direction of thinking. Thus, it is unnecessary to use a set tool; any tool may be helpful for generating a good idea. We propose that the silicon steel plate of the motor is replaced with nano Fe_3O_4 powder.

1. Introduction

Cogging torque[1–9] is the interactive force generated by the relative motion of the rotor magnets and the stator tooth groove of the stacked silicon steel plates in a permanent magnet brushless motor, whose repulsive force depends on the relative position. Therefore, before the motor is electrically excited and rotating, there already exists a periodic torque change called cogging torque, and the ripple torque is its waveform, as shown in Fig. 1. Cogging torque affects the motor's smooth rotation and shortens its life, regardless of whether or not it is powered. Figure 1 shows the stable and unstable points of cogging torque during rotor rotation.

The total torque T of the motor is synthesized from three items, and its equation is expressed as follows:

$$T = \frac{1}{2} i^2 \times \frac{dL}{d\theta} - \frac{1}{2} \varphi^2 \frac{dR}{d\theta} + Ni \frac{d\varphi}{d\theta}, \tag{1}$$

*Corresponding author: e-mail: chlin@nkust.edu.tw
https://doi.org/10.18494/SAM3925

ISSN 0914-4935
https://myukk.org/

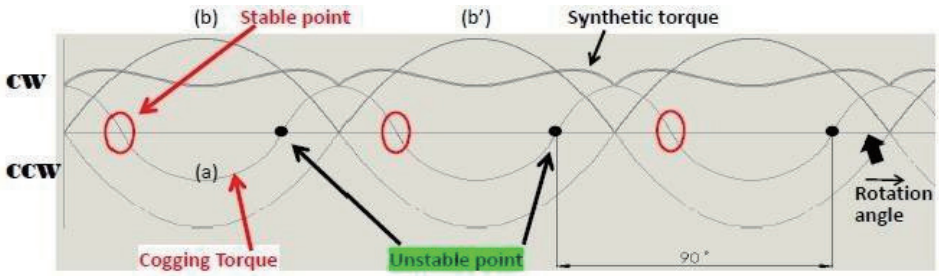

Fig. 1. (Color online) Stable and unstable points of cogging torque during rotor rotation.

$$T = -\frac{1}{2}\varphi_g^2 \frac{dR}{d\theta}. \tag{2}$$

The first item of Eq. (1) is the air gap reluctance. The second item of Eq. (1) is the same as the right-hand side of Eq. (2), that is, the magnetic flux generated by the magnet and the cogging torque caused by the change in the air gap reluctance. The third item of Eq. (1) is the alignment torque generated by the magnetic flux linkage between the coil and the permanent magnet. Since these magnetoresistances are not generated intentionally, they represent forces that must be eliminated or at least minimized so that ripple-free forces can be generated.

The first item in Eq. (1) is generated by the change in the coil self-inductance with the position. According to previous analysis, the self-inductance of the coil is constant. Therefore, the first term in Eq. (1) is zero, and the second term in Eq. (1) is used as the only magnetoresistance component. Owing to its importance, this force is called the cogging force or cogging torque and is expressed as Eq. (2).

Only mutual or aligned force components are considered in the cogging force. In an actual motor, force is generated by reluctance and alignment components, as described in Eq. (2). Equation (2) represents the force that must be eliminated or at least minimized so that a ripple-free force can be produced.

The main component of R is the air gap magnetoresistance Rg. Therefore, if the air-gap reluctance changes with the position, it will produce a twisting force. According to Eq. (2), if the change in air gap reluctance as a function of the position is zero, the cogging force is eliminated. The first and second terms of Eq. (1) cannot be made equal to zero, because the magnetic flux must be maximized to produce the required motor alignment force. Therefore, the cogging force can only be eliminated by making the air gap reluctance constant relative to the position. The goal of this study is to reduce the torque given by the second item in Eq. (1) to zero.

In general, most academics use the relevant dimensions as parameters and substitute them into the Taguchi method to find the best value and then modify it. However, the Taguchi method cannot eliminate the cogging torque perfectly.

According to the literature, there are four ways to reduce cogging torque.

1. By a magnetization method.
2. By a special method based on the ratio of the number of slot teeth to the number of poles.
3. By modifying the shape of the stator's silicon steel plate teeth.
4. By using a slanting slot or magnet skew.

However, none of these methods can eliminate cogging torque. This article is based on the TRIZ book by the Soviet inventor Altshuller,[10–12] (English translation: "Inventor-style task-solving theory", abbreviated to TRIZ). This is also known as the theory of inventive problem solving (TIPS), which can be understood as an inventive problem-solving theory. The calculation rules of TRIZ (ARIZ) suggest that when the ideal innovative solution cannot be obtained by using the contradiction matrix table, a matter-field method should be employed, as shown in Fig. 2.

Different line types can be added to Fig. 2 to make the model more complete.

1. Solid lines represent useful effects, dashed lines represent useful but not sufficient effects, wavy lines represent harmful effects, and arrows represent answer notes.
2. If there are dashed or wavy lines in the substance-field analysis diagram, it means that the system needs innovative improvements.
3. Possible innovative solutions to this problem may also be represented by the substance-field analysis diagram.
4. The stator slot of the motor is skewed to prevent cogging.

Hence, the substance-field analysis diagram is a schematic diagram that models an engineering system as the simplest structure to analyze its irregularities so as to lead to a standard solution to a problem. Following the above guidelines, we can easily think of the material, characteristics, and role of silicon steel in the motor. Then we can examine whether a different material can be used. This idea is the motivation for our research and choice of materials.

2. Characteristics of Magnetic Material

We know from the basic theory of magnetism and the application of magnetic materials that a silicon steel plate is a soft magnetic material that transmits the magnetic circuit in a motor. Magnetic hysteresis curves are usually used to represent the properties of magnetic materials as shown in Fig. 3.

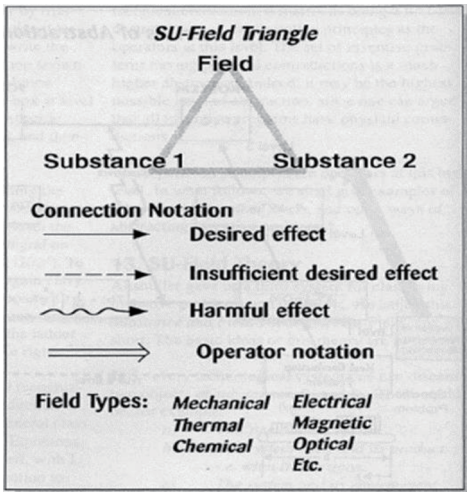

Fig. 2. Procedure of substance-field analysis.

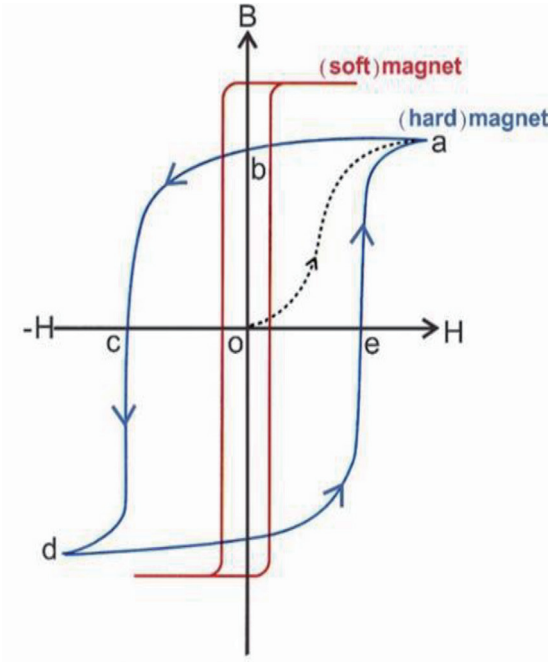

Fig. 3. (Color online) Hysteresis loop of the magnetic material.

Figure 3 shows the change in the magnetic induction strength *B* of an unmagnetized ferromagnetic material placed in an electromagnetic field when it is magnetized by an applied electromagnetic field of strength *H* in the positive and negative directions. The graph shows that when *H* increases gradually from the origin O, the maximum value of *B* for the ferromagnetic material saturates. However, when the applied magnetic field is gradually reduced, the magnetic field path of the ferromagnetic material does not return along the original magnetization curve (dotted line), but changes to the curve a→b→c→d→a. Even if the applied magnetic field strength decreases to zero, the ferromagnetic material still retains its magnetism (remanence) at point b. This magnetic field strength is called remanence, which produces hysteresis. If the reverse electromagnetic field continues to be applied, the same effect as the forward electromagnetic field will induce the magnetization of the ferromagnetic material to reach the saturation point. If the inverse field is reduced to zero, the magnetic strength of the ferromagnetic material is still negative. If the positive magnetic field continues to be applied, the magnetization curve will follow the curve along the points d→e→a, which is a closed curve. This closed curve is called the hysteresis curve.

The hysteresis curve has two important indicators. One is the residual magnetization (remanence), usually represented by *Bs*, which is the magnetic induction strength from point b to O on the graph. The other is the coercivity, usually represented in the unit of Oe or A/m, which is the magnetic field strength (force) from C to O. The hysteresis width of the soft magnetic material (red) is small, whereas the width of the hard magnetic material (blue) is large.

As shown in Fig. 4, superparamagnetism means that when the applied magnetic field increases, the magnetization of some magnetic particles at the nanoscale increases proportionally

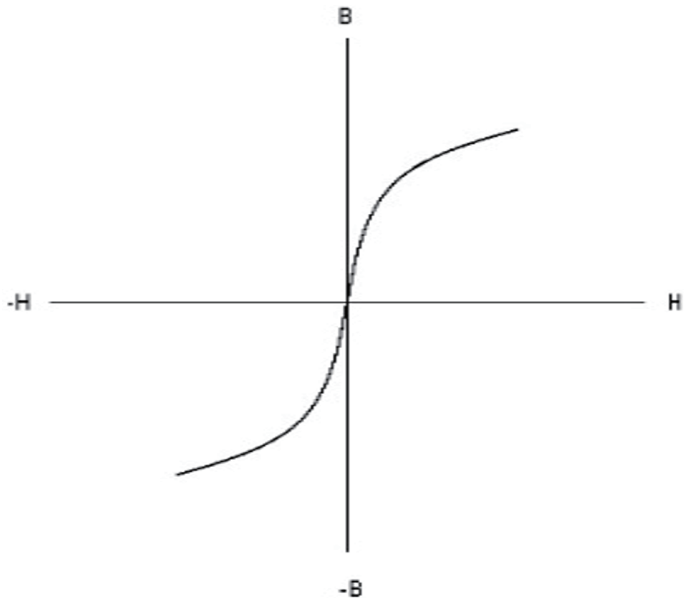

Fig. 4. Superparamagnetism hysteresis curve.

with the strength of the applied magnetic field until it reaches the saturation state. At this time, the magnetization of nanoparticles no longer increases, and the magnetic moments of magnetic particles tend to align neatly in the direction of the applied magnetic field. When the applied magnetic field is removed, the magnetism of the nano-magnetic particles disappears immediately and there is almost no residual magnetism. Without remanence, there is no coercivity. In other words, there is no cogging torque. Nano Fe_3O_4 powder is commonly used as magnetic nanoparticles. These nanoparticles are insoluble in water provided their surface is covered with a layer of a hydrophilic interfacial active agent, enabling them to be stably dispersed in water. Such a solution can be used as a magnetically conductive fluid.

Although these magnetic nanoparticles or magnetic fluids possess excellent superparamagnetic properties, there is no suitable structural design that would allow these materials to be used in the aforementioned motor components.

3. Machining Process of Material and Motor

3.1 Production of nano Fe_3O_4 powder

Nano Fe_3O_4 powder is usually produced by the reaction of Fe^{2+} ions and Fe^{3+} salts under alkaline conditions using the following steps, where the reaction is given by Eq. (3):

$$Fe^{2+} + 2Fe^{3+} + 8OH^{-} \rightarrow Fe_3O_4 + 4H_2O\cdot \tag{3}$$

Step 1: Add 5 g of ferric chloride and 10 g of ferrous chloride to 40 ml of hydrochloric acid solution.

Step 2: Add 40 ml of 2 M sodium hydroxide solution to the resulting solution and stir to precipitate the iron oxide nanoparticles.
Step 3: After adding the sodium hydroxide, set the temperature at 50 °C, stir for 1 h, and leave for 15 min.
Step 4: Place a strong neodymium magnet on the outside of the beaker to extract the iron oxide.
Step 5: Dry the thick iron oxide at 60 °C.
Step 6: Wash the iron oxide solids with deionized water.
Step 7: Wash the iron oxide solids with dilute hydrochloric acid.

Black Fe_3O_4 powder is thus obtained as shown in Fig. 5. In this study, the magnetic powder was measured using a vibrating sample magnetometer (VSM) as shown in Fig. 6. Figure 7 shows the nano Fe_3O_4 powder, which exhibits superparamagnetic hysteresis curves.

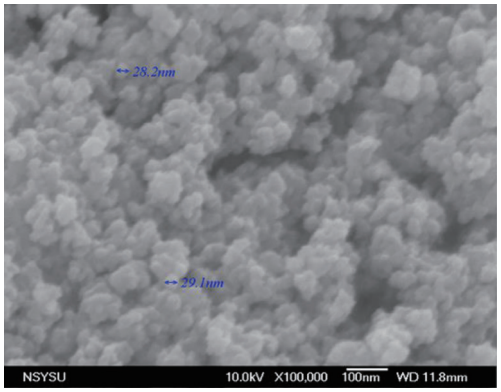

Fig. 5. (Color online) Nano Fe_3O_4 powder observed by electron microscopy.

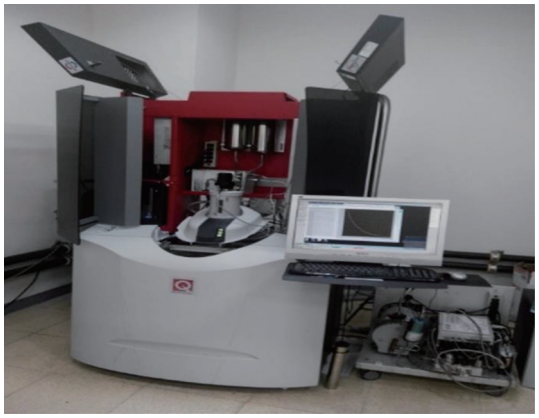

Fig. 6. (Color online) Vibrating sample magnetometer.

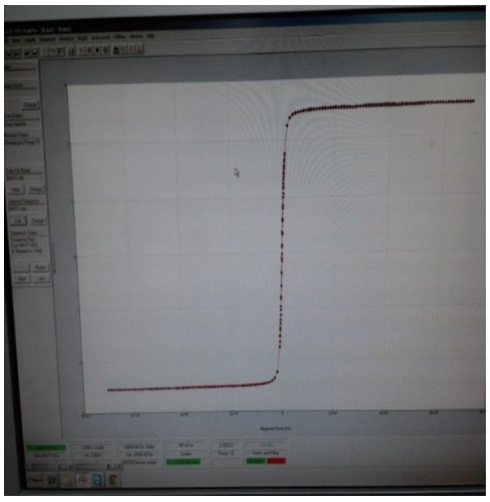

Fig. 7. (Color online) Superparamagnetic hysteresis curves of nano Fe_3O_4 powder.

3.2 Production of motor stator

A superparamagnetic component is applied to an axial-flux permanent magnet brushless motor. The shell of the brushless motor is filled with a magnetic nanomaterial (nano Fe_3O_4 powder). The shell is made of a nonmagnetic material, such as a plastic or polycarbonate material, which does not produce magnetic induction. Figure 8 shows the structure of the shell and Fig. 9 shows the hollow shell filled with the nano Fe_3O_4 powder, which is inserted in the coil center.

According to the winding principle, the coils are wound in a triangular mold to form a single-phase coil string of four coils. Three strings are made in the same way to form a three-phase coil, as shown in Figs. 10 and 11.

In Fig. 10, the three strings of coils (12 strings in total) are wound and supported by a central support block. The outside of the coils is pressed with a stainless-steel band to tighten the coils. Then, the nano Fe_3O_4 powder is placed in the designed triangular shell, which is inserted into the center of the coil as shown in Fig. 11.

Fig. 8. (Color online) Hollow shell.

Fig. 9. (Color online) Hollow shell filled with nano Fe_3O_4 powder.

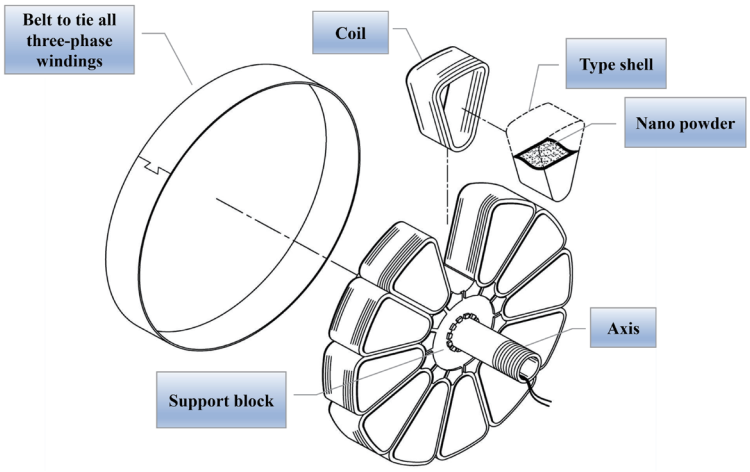

Fig. 10. (Color online) Stator assembly with nano Fe_3O_4 powder and other parts.

Fig. 11. (Color online) Rotor disks and coil stator.

3.3 Assembly process of motor

As shown in Fig. 12, the first (left) rotor disk consists of 16 magnets arranged in an NSNS orientation and a centrally located bearing. The second part is a hollow load ring connected to the left and right rotors with screws. The third part is a coiled disk. Owing to its relatively small radius, it is placed in the center of the hollow load plate. This structure does not interfere with the rotation of the rotor disk. The stator is fixed to the central shaft and the 12 coils are inserted in the center with the nano Fe_3O_4 powder. The outer shell of the powder becomes the stator coil disk. The fourth part is the right rotor disk, which has the same structure as the first rotor disk and is magnetized. The left and right magnetic rotor disks and the clamped load ring are fixed by screws and rotated together by the two bearing rings. The cover is made of transparent plastic, and the nano Fe_3O_4 powder is used as a back-iron. The completed motor prototype is shown in Fig. 13.

4. Simulation Results

In the study, three materials, the silicon steel plate, nano Fe_3O_4 powder, and air, are compared by finite element analysis (FEA), which yielded the results shown in Fig. 14, where the red, green, and black curves represent the results for the silicon steel plate, nano Fe_3O_4 powder, and air, respectively. The response of the electromotive force was greatest for the silicon steel plate, closely followed by the nano Fe_3O_4 powder, then air, which showed about half of the response of the silicon steel plate.

5. Results

The test of the motor prototype carried out in this study is suitable for passive power load testing. A reluctance brake is usually used to increase the load, and various motor data can be measured, including the output current and voltage, output power, speed, and torque efficiency. Table 1 and Fig. 15 show the characteristics of the motor. Because of the large amount of data, only terms 98 to 117 are shown. The optimum efficiency is about 0.7295 (about 73%) for term 106.

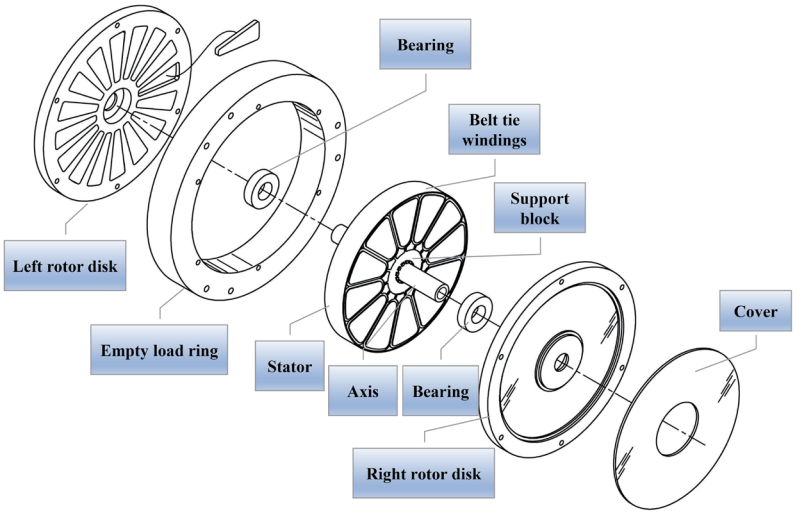

Fig. 12. (Color online) Motor assembly chart.

Fig. 13. (Color online) Finished motor prototype.

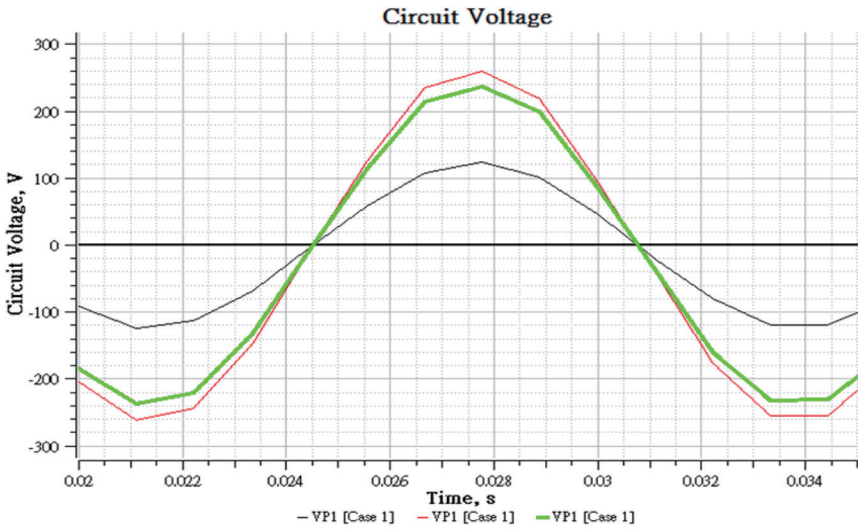

Fig. 14. (Color online) Comparison results of silicon steel plate, nano Fe_3O_4 powder, and air.

Table 1
Results of testing prototype motor.

Term	Input current (A)	Input voltage (V)	Win input	rpm	Torque (Gr/cm)	Efficiency	Output power (W)	Power factor (PF)
98	1.565	47.59	74.379	1001	5230.000	0.7228	53.7635	0.9989
99	1.582	47.58	75.194	999	5247.000	0.7159	53.8306	0.9989
100	1.602	47.58	76.122	996	5280.000	0.7095	54.0065	0.9989
101	1.612	47.57	76.602	995	5342.000	0.7126	54.5858	0.9990
102	1.628	47.57	77.354	992	5391.000	0.7100	54.9204	0.9990
103	1.654	47.57	78.613	989	5583.000	0.7213	56.7044	0.9990
104	1.669	47.56	79.308	987	5601.000	0.7158	56.7721	0.9990
105	1.694	47.55	80.476	983	5673.000	0.7116	57.2689	0.9990
106	1.722	47.55	81.810	980	5930.000	0.7295	59.6806	0.9990
107	1.736	47.55	82.454	978	5862.000	0.7140	58.8759	0.9990
108	1.755	47.54	83.334	975	5914.000	0.7106	59.2159	0.9991
109	1.773	47.54	84.181	972	6000.000	0.7115	59.8922	0.9991
110	1.785	47.53	84.754	971	6116.000	0.7196	60.9873	0.9991
111	1.812	47.52	86.013	968	6156.000	0.7115	61.1965	0.9991
112	1.823	47.52	86.546	965	6336.000	0.7255	62.7907	0.9991
113	1.840	47.52	87.343	964	6331.000	0.7176	62.6761	0.9991
114	1.859	47.51	88.234	962	6363.000	0.7125	62.8622	0.9991
115	1.875	47.51	88.983	959	6507.000	0.7202	64.0843	0.9991
116	1.900	47.50	90.173	956	6556.000	0.7138	64.3649	0.9991
117	1.923	47.49	91.236	954	6616.000	0.7104	64.8181	0.9991

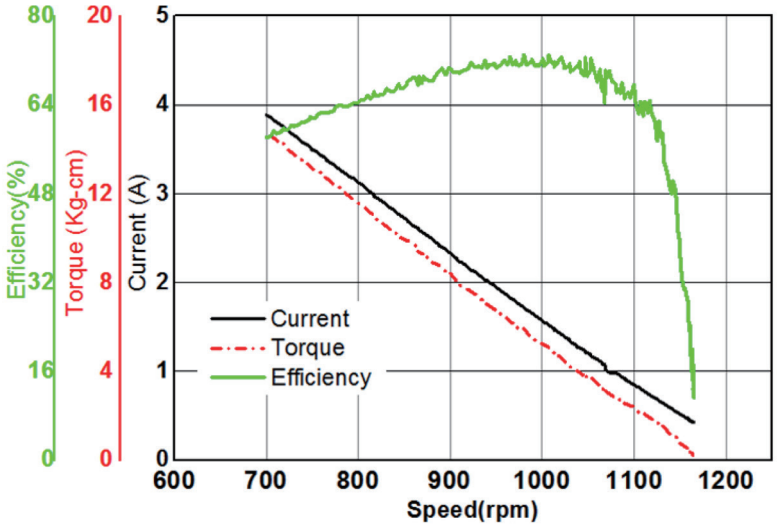

Fig. 15. (Color online) Motor characteristic chart.

The results of this test showed that the center axis of the reluctance brake was not perfectly aligned with the center axis of the motor when they were coupled. Therefore, the efficiency curve in Fig. 15 is not very smooth because of the poor alignment of the motor shaft. The permanent magnet motor designed for this study is an ideal structure; if it is used to manufacture the motor, the following advantages can be expected.

1. The power can be varied as desired. For example, two 500 W motors can provide a power of 1000 W.
2. The air gap, which is the distance between the stator and the rotor and affects the speed and torque, can be easily changed.
3. The numbers of stator slots and rotor poles can be easily changed.
4. The size of the fixed rotor can be easily changed and the thickness of the copper wire can be easily adjusted.

In a 48 V load test, we observed that the highest efficiency was 73% including the efficiency of a driver. This means that after redesigning and replacing the silicon steel plate and air with nano Fe_3O_4 powder in the shell, the overall increase in efficiency will be significant when the problems regarding the ferromagnetic hysteresis of the silicon steel plate, the eddy current losses, and the excess mass of the motor are all resolved.

6. Conclusions

Cogging torque is a product of the magnetic interaction between the poles of the rotor's permanent magnets and the steel laminations of the stator's teeth. In this study, the shell of the brushless motor is filled with nano Fe_3O_4 powder instead of silicon steel plate. The magnetic powder was measured using a vibrating sample magnetometer to verify the characteristic of superparamagnetic hysteresis that exhibits low core loss and high magnetic susceptibility. Three materials, silicon steel plate, nano Fe_3O_4 powder, and air, are compared by finite analysis using JAMEG software. It is found that the maximum efficiency of a brushless motor with nano Fe_3O_4 powder is approximately 73% in a 48 V load test. By applying the proposed nanomaterial in a brushless motor, the cogging torque problem can be solved and losses can be minimized to improve efficiency.

References

1 S. X. Chen, T. S. Low, and B. Bruhl: IEEE Trans. Magn. **34** (1998) 2135. https://doi.org/10.1109/20.706828
2 D. Hanselman: Brushless Permanent Magnet Motor Design (Midpoint Trade Books Inc., New York, 2003) 2nd ed., Chap. 3.
3 S. I. Kim, J. Y. Lee, Y. K. Kim, J. P. Hong, Y. Hur, and Y. H. Jung: IEEE Trans. Magn. **41** (2005) 1796. https://doi.org/10.1109/TMAG.2005.846478
4 B. Wang, G. Xu, Q. Song, and P. Xu: Proc. 2011 6th Int. Forum on Strategic Technology (IEEE 2011) 361–365.
5 L. Y. Hsu, M. C. Tsai, C. J. Chen, and C. F. Wu: Proc. 2005 Int. Conf. Electrical Machines and Systems (IEEE 2005) 2324–2328.
6 C. C. Hwang, S. P. Cheng, and C. M. Chang: IEEE Trans. Magn. **41** (2005) 971. https://doi.org/10.1109/TMAG.2004.842076
7 T. S. Low, S. Chen, and X. Gao: IEEE Trans. Ind. Electron. **48** (2001) 656. https://doi.org/10.1109/41.925593
8 G. S. Altshuller: Creativity As an Exact Science (CRC Press, New York, 1984) 1st ed., Chap. 6.
9 D. Mann: Hands-on Systematic Innovation: for Technical Systems (IFR Press, Frankfurt, 2007) 1st ed., Chap. 3.
10 C. C. Lin, H. H. Lin, and K. C. Huang: Proc. 2016 3rd Int. Conf. Systems and Informatics (ICSAI) (IEEE, 2016) 1072–1076.
11 G. Pahl, W. Beitz, J. Feldhusen, and K. Grote: Engineering Design A Systematic Approach (Springer, 2007) 3rd ed., Chap 8.
12 R. J. Wang, M. J. Kamper, K. Westhuizen, and J. F. Gieras: IEEE Trans. Magn. **41** (2005) 55. https://doi.org/10.1109/TMAG.2004.840183